RESEARCH ARTICLE

Check for updates

Stabilization of copper iodide hybrids with increased strength of ionic bonding for lighting and X-ray imaging†

Qianqian Wang, Haibo Li, [iD] * Jiali Fan, Zhennan Zhou, Hua Tong, Jialin Zhu, Wei Liu [iD] * and Gangfeng Ouyang [iD] *

A new strategy of improving the stability of organic–inorganic hybrid materials by increasing the charge of organic compounds to enhance the strength of ionic bonds has been demonstrated. Based on this method, we have designed and synthesized a series of ionic copper iodide hybrid structures with significantly improved stability and excellent photo/radio-luminescence, showing potential as new solid-state lighting phosphors and X-ray scintillators.

Introduction

Organic metal halides are a class of functional materials which have attracted significant attention due to their excellent optoelectronic properties.[1–10] These materials typically possess the following characteristics: (1) adjustable bandgap: by changing the size and properties of halogen ions or organic cations, the bandgap of the materials can be precisely controlled to meet different application requirements;[11–13] (2) high photoelectric conversion efficiency: some organic metal halides exhibit very high photoelectric conversion efficiency, making them particularly attractive in the field of solar cells;[14,15] (3) low manufacturing cost: this type of materials can be prepared by solution processing method which is more economical and facile compared to the process of other traditional inorganic semiconductor materials.[16–18] However, despite their enormous application prospects in technologies such as photovoltaics and solid-state lighting, stability is one of the main obstacles limiting their commercialization.[19–22] Water, oxygen, and temperature changes in the environment can all lead to the decomposition of these materials and the decrease in the performance, especially under long-term use conditions.[23,24] To address this issue, researchers are exploring various strategies to improve the stability of organic metal halide materials, including: improve packaging technology,

doping and interface engineering, defect management, adopting new device architectures, *etc*.[25–27] Among them, designing new and stable structures is the most direct and fundamental solution for the development of better-performing optoelectronic devices.[28–32]

Previous studies show that ionic metal halide hybrids exhibit higher stability than neutral structures, due to stronger ionic bonds compared to metal–ligand coordinative bonds.[33–36] The strength of ionic bonds is directly related to the number of charges: the larger the magnitude of the charges of the ions, the stronger the electrostatic attraction between them. Thus, larger charges mean stronger ionic bonding. Therefore, by increasing the charge of organic species in the hybrid structures, the stability of whole hybrid compounds can be effectively enhanced. Most reported ionic metal halides have organic ligands with one positive charge.[2] Organic ligands with two positive charges are scarce and difficult to prepare, resulting in limited systematic research on such hybrid materials based on these organics. Designing and synthesizing organic ligands with higher charge numbers, and studying how these high charge organics affect the properties of the final hybrid materials will be an efficient route for the development of stable functional metal halide hybrids. Due to the significant challenges in the synthesis of multi charged organic ligands, it requires the development of new synthesis strategies and methodologies.

Here, we propose a facile method for preparing organic ligands with two positive charges. We used triethylenediamine (ted) as the parent structure, and made modification based on it. Ted has two nitrogen atoms and we performed alkylation reactions on both nitrogen atoms to prepare a series of ted derivatives with two positive charges. A wide range of halogenated hydrocarbons can be used for the synthesis. By reacting

School of Chemical Engineering and Technology, Sun Yat-sen University & Southern Marine Science and Engineering Guangdong Laboratory (Zhuhai), Zhuhai, 519082 Guangdong, P. R. China. E-mail: lihb63@mail.sysu.edu.cn, liuwei96@mail.sysu.edu.cn, cesoygf@mail.sysu.edu.cn

This journal is © the Partner Organisations 2024

Inorg. Chem. Front., 2024, **11**, 7399–7406 | **7399**

these ted derivatives with copper iodide, a new ionic material structure system with zero-dimensional copper iodine discrete clusters as inorganic functional units can be systematically prepared. The synthesized copper halide hybrid structures exhibit both photo- and radio-luminescence and superior stability.

Results and discussion

In this work, three "R-ted-R" (R = alkyl group) organic ligands were successfully synthesized, denoted as L_1, L_2 and L_3 respectively. The synthetic route of the ligands is shown in Fig. S1,† showing that the ligands are ted derivatives substituted by two n-propyl, n-butyl, and n-pentyl groups, respectively. The ligands were obtained by a facile process, in which ted was mixed with the corresponding bromoalkane in acetonitrile solution and the mixture was stirred for two days. More information about the preparation process is provided in Table S1.† The successful syntheses and high purity of the ligands were verified by mass spectrometry (MS) and nuclear magnetic resonance hydrogen spectroscopy (^{1}H-NMR) (Fig. S2–S4,† respectively). Their abbreviations are Pr-ted-Pr, Bu-ted-Bu, and Pen-ted-Pen respectively, and the specific structures of the ligands have been drawn in Fig. S2–S4.†

The obtained ligands were reacted with cuprous iodide by a slow diffusion method, and crystals of three new CuI-based hybrids were synthesized, which were named as compounds **1**, **2** and **3**, respectively. The transparent rod-like crystals of **1–3** were obtained, which emit yellow light under ultraviolet

irradiation (Fig. 1a–c). The transparent crystals are typically suitable for single-crystal X-ray diffraction (SCXRD) analysis and their crystal structures are determined. Specifically, the structure of compound **1** consists of inorganic modules of one $Cu_4I_8{}^{4-}$ and three $CuI_4{}^{3-}$, and six Pr-ted-Pr organic ligands (Fig. 1d). The structure of compound **2** composed of one $Cu_3I_6{}^{3-}$ module and one Bu-ted-Bu ligand (Fig. 1e). While compound **3** possesses four $Cu_3I_6{}^{3-}$ inorganic modules and six Pen-ted-Pen organic ligands (Fig. 1f). The main bond angles and bond lengths data for compounds **1–3** are summarized in Tables S6–11,† respectively. The views of the single-crystal structure of the inorganic modules in compounds **1–3** from different directions are displayed in Fig. 1g–i, respectively. The phase purity of the compounds was studied by powder X-ray diffraction (PXRD). As shown in Fig. 1j–l respectively, all the simulated SCXRD patterns are in good concordance with the corresponding experimental PXRD patterns, indicating that correct structures are exactly figured out and pure phase samples have been prepared. Important crystallographic data of compounds **1–3** are summarized in Table S2,† and the structures were deposited in The Cambridge Crystallographic Data Centre (CCDC) with deposition numbers of 2368508–23685010,† respectively. XPS survey spectra and the Cu 2p, N 1s and I 3d high-resolution XPS spectra of compounds **1–3** are provided in Fig. S5.† The survey spectra illustrate the coexistence of C, N, I, and Cu elements in compounds **1–3**. The distinguished XPS peaks of Cu 2p at 933.0 and 952.9 eV correspond to the signal of monovalent Cu(I), implying the negligible oxidation of Cu(I) during the sample synthesis process.[37]
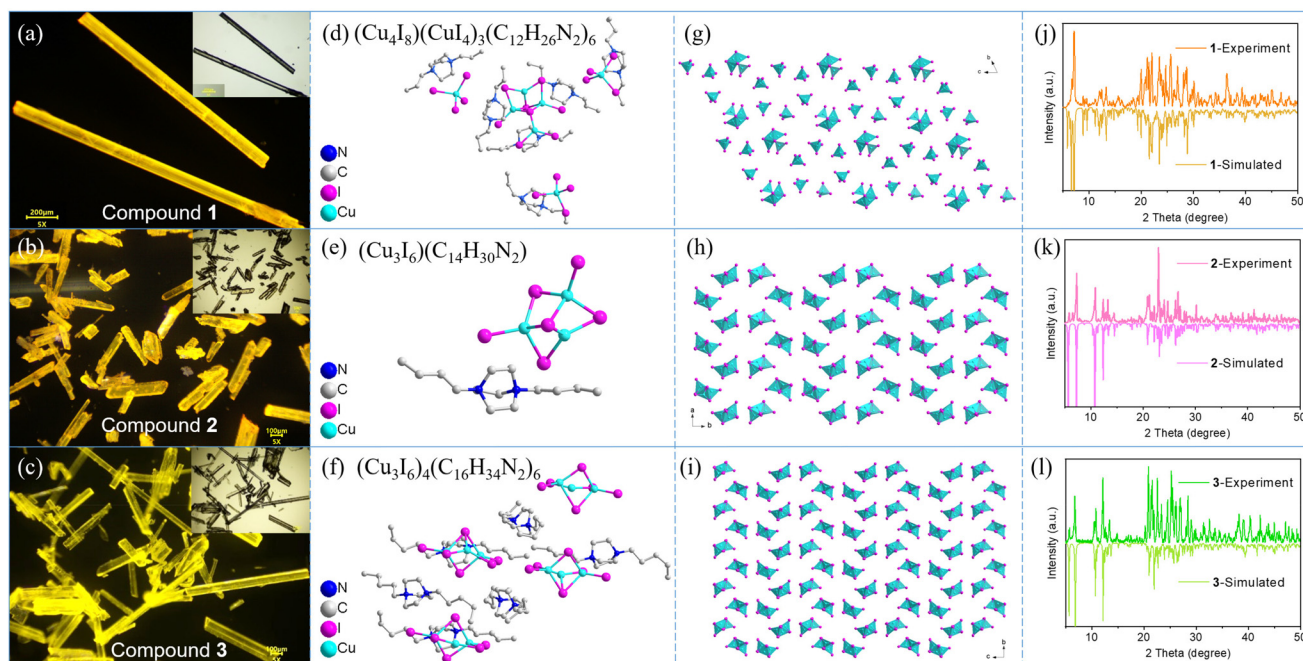

Fig. 1 (a–c) Microscope images of crystals under 365 nm UV light excitation (insets are under transmitted white light), (d–f) schematic diagrams of crystal structure and (g–i) inorganic module views, and (j–l) simulated XRD and experimental PXRD patterns of compound **1**, **2** and **3**, respectively (one H_3O^+ in compound **1**, one K^+ and three CH_3OH in compound **2** are omitted for consistency of the structural formula).

The optical absorption spectra of **1–3** were collected at room temperature and their band gaps are estimated from the optical absorption data by Tauc method. As shown in Fig. S6,† their band gaps are at about 3.3 eV with absorption edges around 400 nm, which are consistent with their cut-off wavelength of the excitation spectra in Fig. 2a–c. Compound **1** has no absorption in the visible light region, which is consistent with its nature of colorless transparent crystal under natural light. While compounds **2** and **3** have blue light absorption in the visible region, resulting in their appearance of yellowish color under natural light. The room-temperature photoluminescence excitation (PLE) and emission (PL) spectra of **1–3** are collected and displayed in Fig. 2. As can be seen, compounds **1–3** exhibit the similar PLE and PL spectra with maxima at around PLE_{max} = 330 nm and PL_{max} = 580 nm, respectively (see details in Table S3†). Their Stokes shifts are around 250 nm (Table S3†). Such a large Stokes shift could prevent self-absorption, making compounds **1–3** well suited as light-emitting materials.[38–40]

The Commission Internationale de l'Eclairage (CIE) chromaticity coordinates are calculated for compounds **1–3** based on their emission spectra, which are listed in Fig. S7.† It's worth noting that, the coordinate of compound **3** (578 nm) at (0.454, 0.510) is close to that of the standard yellow light (575 nm) at (0.479, 0.520). The excitation-dependent PL measurements of compounds **1–3** were investigated and the spectra are displayed in Fig. S8.† As can be seen, though the emission intensities change with the excited energies, the emission ranges and shapes remain the same, indicating that the emission belongs to the single radiative transition mechanism. The luminescence lifetime decay curve of compounds **1–3** at room temperature is

shown in Fig. 2, which was well obtained by double exponential fitting, indicating that different luminescence processes exist in these hybrid materials. The lifetimes of compounds **1–3** are concentrated in the long lifetime range of 0.8–2.5 μs (see Fig. 2 for details), indicating their nature of phosphorescent emission. For their luminescence mechanism, as the cuprous iodide clusters and the organic ligands in these compounds are discrete without the connection of covalent bonds, according to the literature,[41] the organic-ligand-related excited states such as halogen-to-ligand charge transfer (XLCT) or metal-to-ligand charge transfer (MLCT) would be eliminated and the origin of emission could be clearly assigned to the cuprous iodide clusters. Thus, the emission band should be assigned to a triplet "cluster-centered" (³CC) excited state, which has mixed iodide-to-metal charge transfer (³XMCT) and metal-centered transfer (³MC: $d^{10} \rightarrow d^9S^1Cu$).[41] The photoluminescent quantum yields (PLQYs) of these compounds are around 60% (Fig. S9†), which are higher than many other luminescent organic–inorganic hybrid materials.

Thermal stability of the ionic structured compounds **1–3** has been estimated by TG analysis as shown in Fig. 3a–c. The decomposition temperatures (T_{D}) of all structures are higher than 215 °C, which is high among CuI-based organic–inorganic hybrids.[7,42–45] The compounds exhibit a distinct decomposition process with first weight loss of organic ligand at around 220–400 °C and then weight loss of copper iodide over 500 °C. With superior thermal stability, compounds **1–3** maintain their emissive intensity after heating at 100 °C in air for 24 h (Fig. 3e and f). These tests adequately demonstrate that the unique ionic structure brings extraordinary stability to compounds **1–3**.
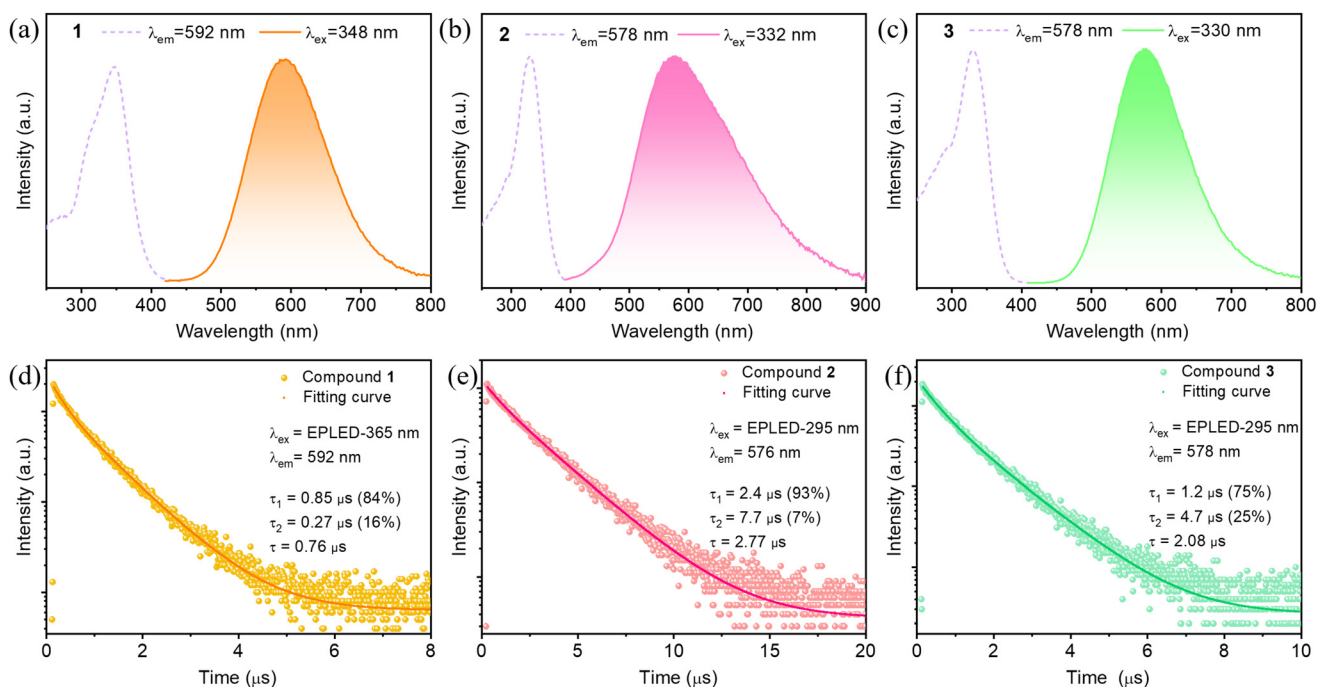

Fig. 2 (a–c) Photoluminescence excitation spectra (dashed line) and emission spectra (solid line), and (d–f) fluorescence lifetime decay curves and their bi-exponential fit curves of compounds **1–3** at room temperature.
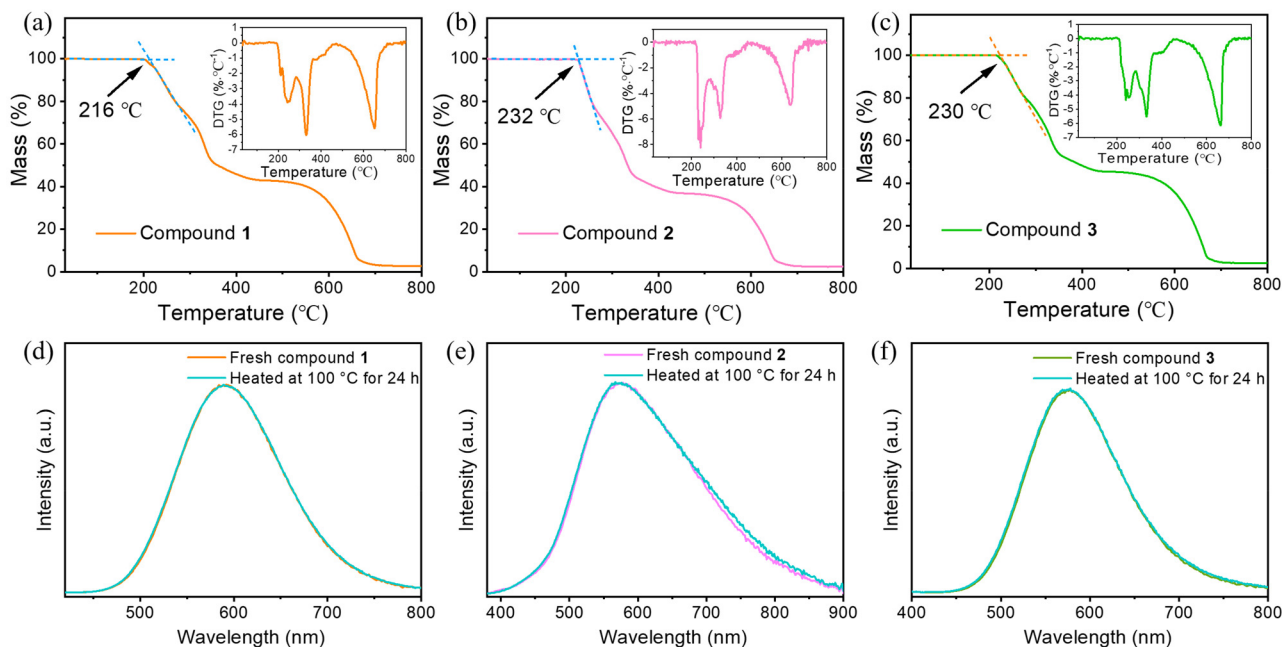
Fig. 3 (a–c) TG and DTG (inset) curves of compounds **1**–**3**. (d–f) Emission intensities of compounds **1**–**3** in fresh state and after heating at 100 °C in air for 24 hours.

Compound **3** is selected for the fabrication of lighting devices to evaluate its suitability as lighting phosphors. Due to the lack of blue light emission, a commercial blue-emitting phosphor BAM (BaMgAl$_{10}$O$_{17}$:Eu) is employed to mix with compound **3** to obtain the white light emitting phosphor.

Different mass ratios of the two compounds (BAM : compound **3**) were adopted, and a white light-emitting phosphor was obtained at the mixed ratio of 1 : 25 according to the PL spectra and CIE coordinates (Fig. 4a and b). Specifically, the CIE coordinate of the mixed phosphor with ratio of 1 : 25
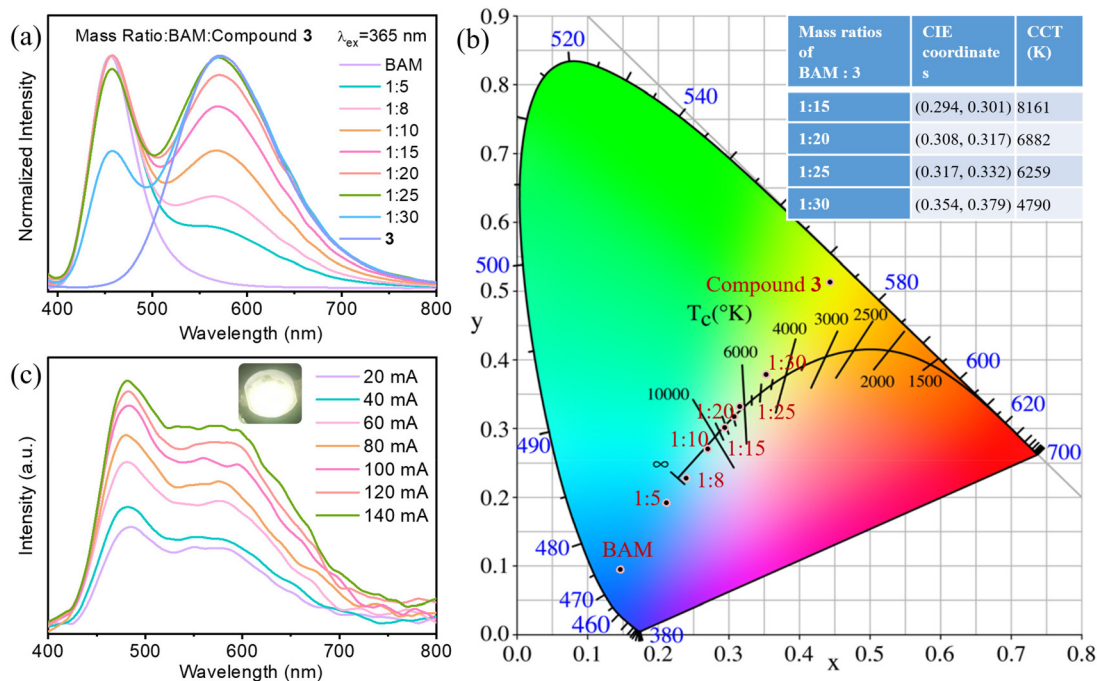
Fig. 4 (a) Normalized PL emission spectra (λ_{ex} = 365 nm) of the mixed phosphors of BAM with compound **3**. (b) Emission spectra of WLED bulb at ratio of 1 : 25 at different currents, inset is the photograph of WLED bulb when energized. (c) CIE coordinate plots of the mixed phosphors of compound **3** and BAM.

7402 | *Inorg. Chem. Front.*, 2024, **11**, 7399–7406

This journal is © the Partner Organisations 2024

(0.32, 0.33) is close to that of pure white light (0.33, 0.33). By encapsulating the mixture of white light-emitting phosphor and UV curing adhesive on a 365 nm UV light-emitting diode (LED) chip, the white LED (WLED) bulb was prepared (inset in Fig. 4c). The emission spectra of the WLED under different currents are obtained, as shown in Fig. 4c. The emission intensity of the WLED gradually increases with the increase of input current. As the shape of the emission spectra barely changes, the CIE coordinates, color rendering index (CRI) and the correlated color temperature (CCT) are maintained at around (0.33, 0.39), 85 and 5220 K, respectively. It can be seen that the WLED has high CRI and good color stability, confirming that compound **3** is a promising LED phosphor alternative. More comparison of WLED performance of compound **3** with other similar luminescent materials is listed in Table S4.†

Compounds **1–3** are soluble in common organic solvents, such as DMF, DMSO, *etc.*, at room temperature, demonstrating their superior solution processability. No luminescence has been observed for the dissolved solution. The sample could be recrystallized by volatilization of the solution, and after it dried out, the luminescent of the samples could be recovered. As shown in the inset of Fig. S7,† a thin film of compound **3** has been prepared by drop-casting **3**@DMF solution on a glass substrate, showing a strong yellow emission under UV light. More importantly, compounds **1–3** have potential applications in X-ray detection and imaging. It is well known that the ability to capture internal structures and details invisible to the naked eye makes X-ray imaging an invaluable tool for diverse applications.[46,47]

The X-ray absorption coefficients of compounds **1–3** and commercial scintillators BGO ($Bi_4Ge_3O_{12}$) were calculated over a wide photon energy range in the XCOM: Photon Cross Sections Database (**https://www.nist.gov/pml/xcom-photon-cross-sections-database**). As shown in Fig. 5a, the X-ray absorp-
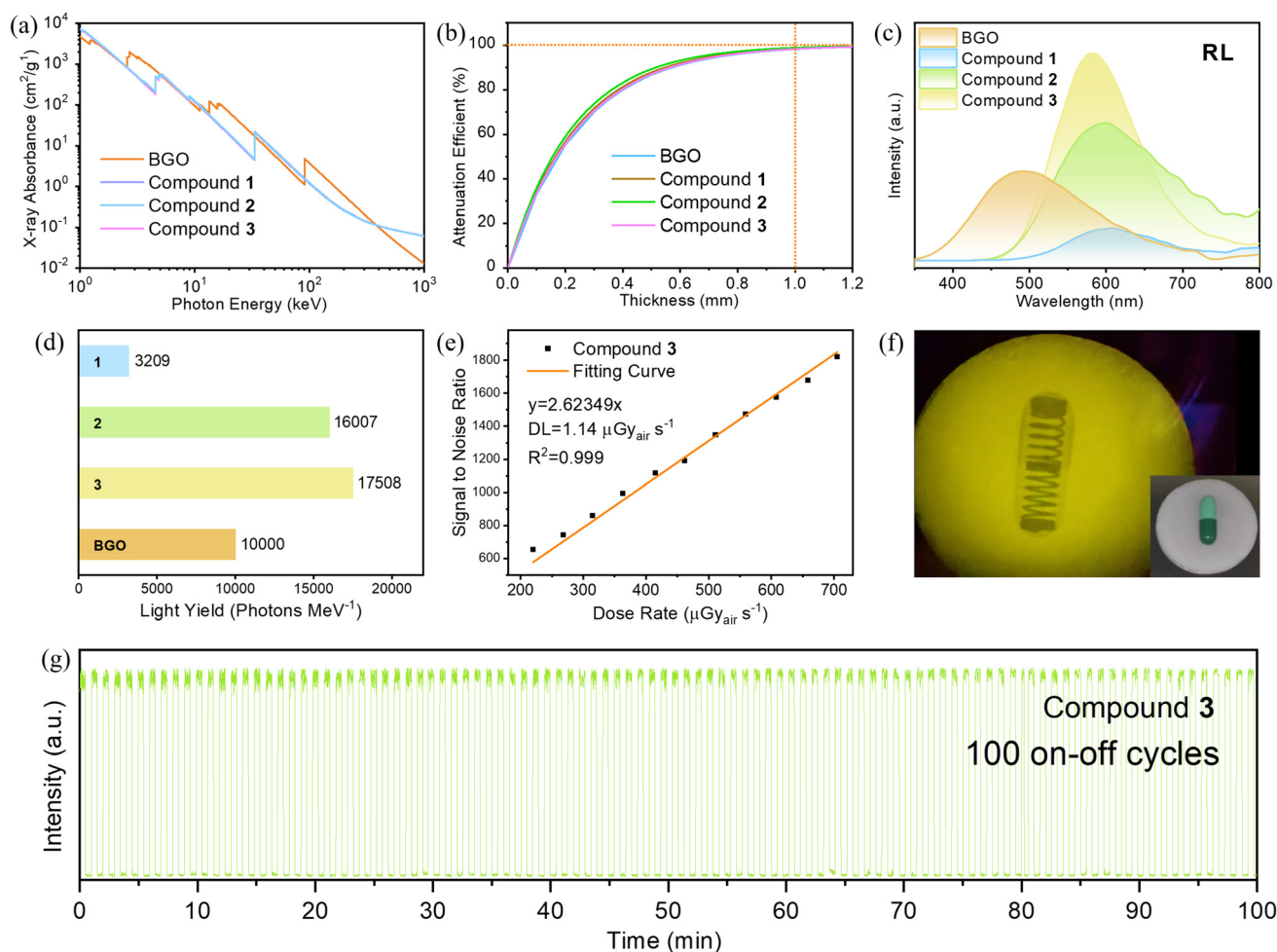

Fig. 5 (a) Functional relationship between the absorption coefficient and photon energy of compounds **1–3** and BGO scintillators. (b) Calculated X-ray attenuation efficiencies of compounds **1–3** and BGO as a function of scintillator thickness. (c) RL spectra of BGO and compounds **1–3**. (d) Comparison of light yields between compounds **1–3** and BGO. (e) Recorded SNR values of compound **3** as a function of dose rate. The detection limit can be defined as the value at the SNR is 3. (f) X-ray image of **3**@PDMS flexible film attaching a capsule containing a spring, inset is the optical image of **3**@PDMS flexible film before X-ray exposure. (g) X-ray tolerance of compound **3** against repeated X-ray irradiation (dose rate: 705 µGy$_{air}$ s^{-1}, with an interval of 30 s).

This journal is © the Partner Organisations 2024

Inorg. Chem. Front., 2024, **11**, 7399–7406 | **7403**

tion coefficients of compounds **1–3** are higher than commercial scintillators in the medical digital radiography region of 40–60 keV and at the characteristic peak of tungsten target X-ray source of 8 keV.[41] Fig. 5b shows the X-ray attenuation efficiency of compounds **1–3** and BGO as a function of thickness at an X-ray photon energy of 8 keV, which are near 100% at a thickness of 1 mm and calculated to be 98.4%, 98.8%, 98.2% and 98.2% respectively. Further, radioluminescence (RL) spectra of compounds **1–3** were estimated in comparison with commercial X-ray scintillator BGO. As shown in Fig. 5c, both the emission intensities of compound **2** and **3** are stronger than that of BGO. Stead-state X-ray-to-light conversion efficiencies are quantified as X-ray light yield based on a reference value of BGO (10 000 photons per MeV), and are calculated by the RL spectra integrated area and the X-ray attenuation efficiency. The relative X-ray light yield of compounds **1–3** are estimated to be 3209, 16 007 and 17 508 photons per MeV respectively (Fig. 5d).[48–51] The light yield of compound **3** is about 1.7 times that of commercial BGO, indicating its great application prospect as X-ray scintillators.

To demonstrate their application for X-ray imaging, compound **3** was chosen to carry out the application tests of X-ray imaging. The radioluminescence (RL) spectra of compound **3** were tested at different X-ray dose rates. As shown in Fig. S10,† the emission intensity increases linearly with the increase of dose rate, and the dose rate-SNR (signal-to-noise ratio) linear curve of the sample was obtained from it by linear fitting, as shown in Fig. 5e. The detection limit of compound **3** is calculated to be 1.14 μGy_{air} s^{-1} under a SNR of 3, which is approximately 4 times lower than the standard dose for medical X-ray examinations (5.5 μGy_{air} s^{-1}).[52] The comparison of X-ray scintillator performance of compound **3** with some similar materials is listed in Table S5.† Additionally, the high robustness of compound **3** to X-ray irradiation was demonstrated, as no noticeable decline was observed during repeated X-ray irradiation (705 μGy_{air} s^{-1}) at 30-second intervals for 100 on–off cycles (Fig. 3g). The above results demonstrate that the compound **3** has excellent chemical stability and low detection limit, manifesting an ideal scintillator material for X-ray imaging. Flexible scintillator screens can be fabricated by combining the high-performance compound **3** with rubber-like, soft, and deformable polydimethylsiloxane (PDMS), as illustrated in the inset of Fig. 5f. Specifically, compound **3** and PDMS were mixed uniformly and then dropped on the glass substrate, and then a thin film with uniform thickness was prepared by spin coating. The spin-coated films can be peeled off the glass substrate after curing at 120 °C overnight. As shown in Fig. 5f, a capsule containing a spring was placed in front of the film and a clear spring image was displayed under X-ray irradiation, indicating its good application prospect of X-ray imaging.

Conclusions

In summary, a series of ionic copper iodide structures with discrete inorganic function motifs have been designed and synthesized, displaying the features of high luminescence and improved stability. Benefiting from the unique doubly charged ionic ligands structure, compounds **1–3** possess excellent stability with decomposition temperature above 215 °C. The WLED based on compound **3** also has good stability under varied currents with a high color rendering index of 85, demonstrating its great application prospect in the field of solid state lighting. In addition, their applications in X-ray scintillators have also been investigated. Compound **3** was found to have low detection limit and good stability under X-ray irradiation, which was selected to fabricate the film. A clear image can be seen under X-ray irradiation, demonstrating that the **3**@PDMS scintillator screen have great application prospect in flexible X-ray detection fields.

Author contributions

Q. W. carried out the experiment and wrote the manuscript. H. L. helped process the data and revise the manuscript. J. F. and Z. Z. carried out the structural characterizations and optical measurements. H. T. and J. Z. helped the tests of WLED bulb. W. L. and G. O. revised the manuscript and supervised the findings of this work. All of the authors discussed the results and contributed to the final manuscript.

Data availability

Further experimental details, characterization data, summary of optical properties and X-ray crystallographic data are available in the ESI.†

Conflicts of interest

There are no conflicts to declare.

Acknowledgements

References

1 C. Wang, S. Chen, J. Jie, C. Tian, R. Jia, X. Wu, X. Zhang and X. Zhang, Metal Halide Perovskite Single Crystals toward Electroluminescent Applications, *Adv. Funct. Mater.*, 2024, 2401189.

2 H. Li, Y. Lv, Z. Zhou, H. Tong, W. Liu and G. Ouyang, Coordinated Anionic Inorganic Module – An Efficient Approach Towards Highly Efficient Blue–Emitting Copper

7404 | *Inorg. Chem. Front.*, 2024, **11**, 7399–7406

This journal is © the Partner Organisations 2024

Halide Ionic Hybrid Structures, *Angew. Chem., Int. Ed.*, 2021, **61**, e202115225.

3 L. P. Ravaro, K. P. Zanoni and A. S. de Camargo, Luminescent Copper(ɪ) complexes as promising materials for the next generation of energy-saving OLED devices, *Energy Rep.*, 2020, **6**, 37–45.

4 J. Troyano, F. Zamora and S. Delgado, Copper(ɪ)–iodide cluster structures as functional and processable platform materials, *Chem. Soc. Rev.*, 2021, **50**, 4606–4628.

5 B. Zhou, Z. Qi, M. Dai, C. Xing and D. Yan, Ultralow–loss optical waveguides through balancing deep-blue TADF and orange room temperature phosphorescence in hybrid antimony halide microstructures, *Angew. Chem.*, 2023, **135**, e202309913.

6 Y. Lin, S. Liu and D. Yan, Flexible Crystal Heterojunctions of Low-Dimensional Organic Metal Halides Enabling Color-Tunable Space-Resolved Optical Waveguides, *Research*, 2023, **6**, 0259.

7 W. Liu, Y. Fang, G. Z. Wei, S. J. Teat, K. Xiong, Z. Hu, W. P. Lustig and J. Li, A Family of Highly Efficient CuI-Based Lighting Phosphors Prepared by a Systematic, Bottom-up Synthetic Approach, *J. Am. Chem. Soc.*, 2015, **137**, 9400–9408.

8 H. Li, J. Yang, Q. Wang, H. Tong, J. Zhu, W. Liu and G. Ouyang, Ligand Detachment—New Insight into the Mechanochromic Luminescence Mechanism of Copper Iodide Complexes with Thermally Activated Delayed Fluorescence, *Adv. Opt. Mater.*, 2024, 2400364.

9 B. Li, Y.-Y. Liu, P. Luo, Y.-R. Liu, Y.-J. Chen, K. Li and S.-Q. Zang, Multi-stimuli-responsive aggregation-induced emission copper iodide cluster, *Sci. China: Chem.*, 2024, **67**, 1193–1197.

10 X.-Q. Liang, R. K. Gupta, Y.-W. Li, H.-Y. Ma, L.-N. Gao, C.-H. Tung and D. Sun, Structural Diversity of Copper(ɪ) Cluster-Based Coordination Polymers with Pyrazine-2-thiol Ligand, *Inorg. Chem.*, 2020, **59**, 2680–2688.

11 C. Zhou, L. J. Xu, S. Lee, H. Lin and B. Ma, Recent Advances in Luminescent Zero-Dimensional Organic Metal Halide Hybrids, *Adv. Opt. Mater.*, 2021, **9**, 2001766.

12 S. Wang, E. E. Morgan, S. Panuganti, L. Mao, P. Vishnoi, G. Wu, Q. Liu, M. G. Kanatzidis, R. D. Schaller and R. Seshadri, Ligand control of structural diversity in luminescent hybrid copper(ɪ) iodides, *Chem. Mater.*, 2022, **34**, 3206–3216.

13 Y. Lv, J. Yang, H. Li, W. Liu and G. Ouyang, Molecular design towards efficient light-emitting copper(ɪ) halide mononuclear hybrids, *Mater. Adv.*, 2024, **5**, 1234–1239.

14 Y. Jiang, T.-F. Xu, H.-Q. Du, M. U. Rothmann, Z.-W. Yin, Y. Yuan, W.-C. Xiang, Z.-Y. Hu, G.-J. Liang and S.-Z. Liu, Organic-inorganic hybrid nature enables efficient and stable CsPbI$_3$-based perovskite solar cells, *Joule*, 2023, **7**, 2905–2922.

15 H. Meddeb, M. Götz-Köhler, N. Neugebohrn, U. Banik, N. Osterthun, O. Sergeev, D. Berends, C. Lattyak, K. Gehrke and M. Vehse, Tunable photovoltaics: adapting solar cell

technologies to versatile applications, *Adv. Energy Mater.*, 2022, **12**, 2200713.

16 W. Liu, Y. Fang and J. Li, Copper Iodide Based Hybrid Phosphors for Energy-Efficient General Lighting Technologies, *Adv. Funct. Mater.*, 2018, **28**, 1705593.

17 W. Liu, K. Zhu, S. J. Teat, B. J. Deibert, W. Yuan and J. Li, A mechanochemical route toward the rational, systematic, and cost-effective green synthesis of strongly luminescent copper iodide based hybrid phosphors, *J. Mater. Chem. C*, 2017, **5**, 5962–5969.

18 H. Tong, Z. Zhou, Y. Lv, H. Li, W. Liu and G. Ouyang, Copper(ɪ) iodide organic–inorganic hybrid luminescent inks for anti-counterfeiting application, *Mater. Adv.*, 2023, **4**, 481–485.

19 T. He, Y. Jiang, X. Xing and M. Yuan, Structured perovskite light absorbers for efficient and stable photovoltaics, *Adv. Mater.*, 2020, **32**, 1903937.

20 J.-J. Wang, L.-Z. Feng, G. Shi, J.-N. Yang, Y.-D. Zhang, H. Xu, K.-H. Song, T. Chen, G. Zhang and X.-S. Zheng, High efficiency warm-white light-emitting diodes based on copper–iodide clusters, *Nat. Photonics*, 2024, **18**, 200–206.

21 C. Xing, Z. Qi, B. Zhou, D. Yan and W. H. Fang, Solid–State Photochemical Cascade Process Boosting Smart Ultralong Room-Temperature Phosphorescence in Bismuth Halides, *Angew. Chem.*, 2024, e202402634.

22 Y. Fang, W. Liu, S. J. Teat, G. Dey, Z. Shen, L. An, D. Yu and L. Wang, D. M. O'Carroll and J. Li, A Systematic Approach to Achieving High Performance Hybrid Lighting Phosphors with Excellent Thermal-and Photostability, *Adv. Funct. Mater.*, 2017, **27**, 1603444.

23 S. Fang, B. Zhou, H. Li, H. Hu, H. Zhong, H. Li and Y. Shi, Highly Reversible Moisture-Induced Bright Self-Trapped Exciton Emissions in a Copper-Based Organic-Inorganic Hybrid Metal Halide, *Adv. Opt. Mater.*, 2022, **10**, 2200605.

24 X. W. Kong, L. X. Wu, X. Yang, D. Y. Wang, S. X. Wang, S. Y. Li, C. Y. Yue, F. Yu and X. W. Lei, Enhancing the Water-Stability of 1D Hybrid Manganese Halides by a Cationic Engineering Strategy, *Adv. Opt. Mater.*, 2024, 2302710.

25 H. Tong, H. Li, Z. Zhou, Cidanpuchi, F. Wang and W. Liu, Strategies for optimizing the luminescence and stability of copper iodide organic–inorganic hybrid structures, *New J. Chem.*, 2021, **45**, 10989–10996.

26 S. Ye, H. Rao, M. Feng, L. Xi, Z. Yen, D. H. L. Seng, Q. Xu, C. Boothroyd, B. Chen and Y. Guo, Expanding the low-dimensional interface engineering toolbox for efficient perovskite solar cells, *Nat. Energy*, 2023, **8**, 284–293.

27 C. Zang, M. Xu, L. Zhang, S. Liu and W. Xie, Organic–inorganic hybrid thin film light-emitting devices: interfacial engineering and device physics, *J. Mater. Chem. C*, 2021, **9**, 1484–1519.

28 H. Li, Y. Lv, Y. Tan, J. Yang, W. Liu and G. Ouyang, Ultrastable Copper Iodide Hybrid with Intrinsic Greenish White-Light Emission by Incorporating an Anionic Inorganic Functional Unit into an Extended Structure, *Inorg. Chem.*, 2024, **63**, 9326–9331.

This journal is © the Partner Organisations 2024

Inorg. Chem. Front., 2024, **11**, 7399–7406 | **7405**

29 H. Tong, H. Li, H. Li, Cidanpuchi, F. Wang and W. Liu, Incorporation of an Emissive Cu_4I_4 Core into Cross-Linked Networks: An Effective Strategy for Luminescent Organic–Inorganic Hybrid Coatings, *Inorg. Chem.*, 2021, **60**, 15049–15054.

30 X. Fan, F. Yuan, J. Wang, Z. Cheng, S. Xiang, H. Yang and Z. Zhang, Structural Isomerization in Cu(ı) Clusters: Tracing the Cu Thermal Migration Paths and Unveiling the Structure-Dependent Photoluminescence, *CCS Chem.*, 2023, **5**, 350–360.

31 S. Yuan, S.-S. Liu and D. Sun, Two isomeric $[Cu_4I_4]$ luminophores: solvothermal/mechanochemical syntheses, structures and thermochromic luminescence properties, *CrystEngComm*, 2014, **16**, 1927–1933.

32 S. Yuan, H. Wang, D.-X. Wang, H.-F. Lu, S.-Y. Feng and D. Sun, Reactant ratio-modulated six new copper(ı)–iodide coordination complexes based on diverse [CumIm] aggregates and biimidazole linkers: syntheses, structures and temperature-dependent luminescence properties, *CrystEngComm*, 2013, **15**, 7792–7802.

33 W. Liu, K. Zhu, S. J. Teat, G. Dey, Z. Shen, L. Wang, D. M. O'Carroll and J. Li, All-in-one: achieving robust, strongly luminescent and highly dispersible hybrid materials by combining ionic and coordinate bonds in molecular crystals, *J. Am. Chem. Soc.*, 2017, **139**, 9281–9290.

34 H. Tong, H. Li, Z. Zhou, F. Wang and W. Liu, Strategies for optimizing the luminescence and stability of copper iodide organic–inorganic hybrid structures, *New J. Chem.*, 2021, **45**, 10989–10996.

35 H. Tong, C. Xu and W. Liu, A highly luminescent and stable copper halide ionic hybrid structure with an anionic $CuBr_2(tpp)_2$ module, *J. Mater. Chem. C*, 2021, **9**, 12530–12534.

36 W. Liu, Z. Zhou, H. Li, Y. Lv, H. Tong, J. Zhu and G. Ouyang, New Strategy for Optimizing the Properties of Copper Halide Organic-Inorganic Hybrid Lighting–emitting Materials, *Chem. – Eur. J.*, 2022, **28**, e202202478.

37 D. Liang, Z. Sun, S. Lu, J. Zhao, Y. Zhou, K. An and Z. Zang, Solvent-Free Grinding Synthesis of Hybrid Copper Halides for White Light Emission, *Inorg. Chem.*, 2023, **62**, 7296–7303.

38 F. Fang, Y. Gao and L. Luo, Mitochondrion-anchoring AIEgen with Large Stokes Shift for Imaging-guided Photodynamic Therapy, *Chem. Res. Chin. Univ.*, 2021, **37**, 137–142.

39 M. Jiang, X. Gu, J. W. Lam, Y. Zhang, R. T. Kwok, K. S. Wong and B. Z. Tang, Two-photon AIE bio-probe with large Stokes shift for specific imaging of lipid droplets, *Chem. Sci.*, 2017, **8**, 5440–5446.

40 X. Zhang, Y. Liu, C.-H. Kuan, L. Tang, T. D. Krueger, S. Yeasmin, A. Ullah, C. Fang and L.-J. Cheng, Highly fluo-

rescent nitrogen-doped carbon dots with large Stokes shifts, *J. Mater. Chem. C*, 2023, **11**, 11476–11485.

41 S.-L. Li, F.-Q. Zhang and X.-M. Zhang, An organic-ligand-free thermochromic luminescent cuprous iodide trinuclear cluster: evidence for cluster centered emission and configuration distortion with temperature, *Chem. Commun.*, 2015, **51**, 8062–8065.

42 C. Xing, B. Zhou, D. Yan and W. H. Fang, Integrating Full-Color 2D Optical Waveguide and Heterojunction Engineering in Halide Microsheets for Multichannel Photonic Logical Gates, *Adv. Sci.*, 2024, **11**, 2310262.

43 K. R. Kyle, C. K. Ryu, P. C. Ford and J. A. DiBenedetto, Photophysical studies in solution of the tetranuclear copper(ı) clusters $Cu_4I_4L_4$ (L = pyridine or substituted pyridine), *J. Am. Chem. Soc.*, 1991, **113**, 2954–2965.

44 P. C. Ford, E. Cariati and J. Bourassa, Photoluminescence Properties of Multinuclear Copper(ı) Compounds, *Chem. Rev.*, 1999, **99**, 3625–3648.

45 C. Xing, Z. Qi, B. Zhou, D. Yan and W. H. Fang, Solid–State Photochemical Cascade Process Boosting Smart Ultralong Room–Temperature Phosphorescence in Bismuth Halides, *Angew. Chem.*, 2024, **136**, e202402634.

46 J. Qiu and X. Liu, A copper-iodide cluster microcube-based X-ray scintillator, *Light: Sci. Appl.*, 2023, **12**, 241.

47 Q. C. Peng, Y. B. Si, J. W. Yuan, Q. Yang, Z. Y. Gao, Y. Y. Liu, Z. Y. Wang, K. Li, S. Q. Zang and B. Z. Tang, High Performance Dynamic X-ray Flexible Imaging Realized Using a Copper Iodide Cluster-Based MOF Microcrystal Scintillator, *Angew. Chem.*, 2023, **135**, e202308194.

48 Z.-Z. Zhang, J.-H. Wei, J.-B. Luo, X.-D. Wang, Z.-L. He and D.-B. Kuang, Large-Area Laminar TEA_2MnI_4 Single-Crystal Scintillator for X-ray Imaging with Impressive High Resolution, *ACS Appl. Mater. Interfaces*, 2022, **14**, 47913–47921.

49 J.-W. Yuan, Q.-C. Peng, J.-C. Fu, Q. Yang, Z.-Y. Gao, Z.-Y. Wang, K. Li, S.-Q. Zang and B. Z. Tang, Highly Efficient Stable Luminescent Radical-Based X-ray Scintillator, *J. Am. Chem. Soc.*, 2023, **145**, 27095–27102.

50 Q. Kong, X. Jiang, Y. Sun, J. Zhu and X. Tao, Yellow-emissive organic copper(ı) halide single crystals with $[Cu_4I_4]$ cubane unit as efficient X-ray scintillators, *Inorg. Chem. Front.*, 2024, **11**, 3028–3035.

51 Y. Wang, W. Zhao, Y. Guo, Y. Hu, C. Peng, L. Li, Y. Wei, Z. Wu, W. Xu, X. Li, Y. D. Suh, X. Liu and W. Huang, Efficient X-ray luminescence imaging with ultrastable and eco-friendly copper(ı)-iodide cluster microcubes, *Light: Sci. Appl.*, 2023, **12**, 155.

52 H. Wei, Y. Fang, P. Mulligan, W. Chuirazzi, H.-H. Fang, C. Wang, B. R. Ecker, Y. Gao, M. A. Loi, L. Cao and J. Huang, Sensitive X-ray detectors made of methylammonium lead tribromide perovskite single crystals, *Nat. Photonics*, 2016, **10**, 333–339.